Global patterns of tropical forest fragmentation

Franziska Taubert[§*], Rico Fischer[§], Jürgen Groeneveld[#,§], Sebastian Lehmann[§], Michael S. Müller[§], Edna Rödig[§], Thorsten Wiegand[§,†], Andreas Huth[§,†,‡]

[§]Helmholtz Centre for Environmental Research GmbH – UFZ, Department of Ecological Modelling, Permoserstrasse 15, 04318 Leipzig, Germany

[#]TU Dresden, Institute of Forest Growth and Forest Computer Sciences, PO 1117, 01735 Tharandt, Germany

[†]German Centre for Integrative Biodiversity Research (iDiv) Halle-Jena-Leipzig, Deutscher Platz 5e, 04103 Leipzig, Germany

[‡]University Osnabrueck, Institute of Environmental Systems Research, Barbarastrasse 12, 49076 Osnabrueck, Germany

*corresponding author

This manuscript provides the accepted manuscript version (9 January 2018).

The published article can be found on

https://www.nature.com/articles/nature25508 (online 14 February 2018)

Nature volume 554, pages 519–522 (22 February 2018)

DOI 10.1038/nature25508

SharedIt http://rdcu.be/GYE6 (read-only access)

Pubmed ID 29443966

Remote sensing allows for the quantification of global tropical deforestation with high spatial resolution[1,2]. This in-depth mapping enabled us to achieve substantial advances in the analysis of continental-wide fragmentation of tropical forests[1-4]. We identified roughly 130 million forest fragments in three continents that show surprisingly similar power law size and perimeter distributions as well as fractal dimensions. Power law distributions[5-7] have been observed in many natural phenomena[8,9] such as wild fires, landslides and earth quakes. The principles of percolation theory[7,10,11] provide one explanation for the observed patterns and suggest that forest fragmentation is close to the critical point of percolation. Simulation modelling supports this hypothesis. The observed patterns do not only emerge from random deforestation which can be described by percolation theory[10,11] but also from a wide range of deforestation and forest recovery regimes. Predictions of our models outline that additional forest loss will strongly increase the total number of forest fragments (maximum by factor 33 over 50 years while decreasing their size), and that this consequence can be partly mitigated by reforestation and forest protection.

Tropical forests play a key role in the global carbon cycle[12] and harbour more than half of the species worldwide[13]. Increases in agriculture, logging and urban growth during the past decades caused unprecedented losses of tropical forest[14,15] with annual deforestation rates reaching about 0.5% since the 1990's[1]. Deforestation rates differ between continents[1] with hot spots mainly concentrated in Asia[14] and Brazil[14] (Tab. 1). A reduction of forested area goes hand in hand with fragmentation where forest patches split up into several smaller ones[16]. The increasing availability of high-resolution satellite imagery now allows for in-depth mapping of global deforestation[1-4] and for a detailed analysis of the spatial pattern of the remaining forest.

Table 1: Derived features of continental-scale fragmentation of tropical forests. All features were calculated based on a high-resolution forest cover map[2].

	America[a]	Africa[a]	Asia-Australia[a]	Theory[f]
Forest area (Mha)	940	577	391	
Number of fragments (N)	55,558,018	44,851,251	30,556,204	
Mean (median) size of fragments (ha)	17 (0.09)	13 (0.09)	13 (0.09)	
Forest area (%) of fragments < 10,000 ha	11.2	9.9	9.2	
Fragment size scaling[b,c] (τ)	1.90	1.98	1.92	2.05
Fractal dimension[b,d] (d_f)	1.92	1.87	1.87	1.89
Perimeter scaling[b,e] (κ)	2.16	2.23	2.21	2.14

[a]Annual gross deforestation rates[1] of 0.51% (America), 0.37% (Africa) and 0.62% (Asia-Australia) for years 2000-2010.

[b]See Methods for details. The term 'scaling' refers to the exponent of the fitted power law distributions. The calculation of fragment size and perimeter scaling is based on n = 55.5 million (America), n = 44.8 million (Africa) and n = 30.5 million (Asia-Australia) fragments.

[c]Pearson's correlation coefficients (R) and standard errors (ε) are: R^2 = 0.96 and ε = 0.0011 (America), R^2 = 0.956 and ε = 0.0017 (Africa), R^2 = 0.958 and ε = 0.0022 (Asia-Australia). Deviations from the theoretical expectation trace back to the finite area of the continents.

[d]The fractal dimension is based on the analysis of n = 8 different grid sizes, see Methods for details. The estimate of the fractal dimension is not affected by landscape area.

[e]Pearson's correlation coefficients (R) and standard errors (ε) are: R^2 = 0.952 and ε = 0.00082 (America), R^2 = 0.931 and ε = 0.0011 (Africa), R^2 = 0.938 and ε = 0.0015 (Asia-Australia).

[f]Theoretical values according to percolation theory[10,11] (near the critical point).

Here we used percolation theory[10,11] as a framework for analysing current fragmentation structures in tropical and sub-tropical America, Africa and Asia-Australia on a high-resolution forest cover map[2] (approx. 21 billion pixels, each 30 m × 30 m). Based on a clustering algorithm, we counted and analysed the size and perimeter distribution of all detectable forest fragments separately for each continent, and determined the fractal dimension of the fragmented landscape (Tab. 1). In total, we identified more than 130 million forest fragments across all continents ranging in size over eleven orders of magnitude up to 427 Mha. South America's largest forest fragment in the Amazon spans about 45% of its total forest area, whereas the largest fragment on Borneo in Asia covers only 18% of the forest.

We expected largely different fragmentation structures among continents due to different land use practices[14]. Unexpectedly, we observed strikingly similar fragment size distributions (Fig. 1) that could be described by power laws[5-7] with almost identical exponents (Tab. 1). About 10% of continental forest area is made up of forest fragments smaller than 10,000 ha (11.2% for America, 9.9% for Africa and 9.2% for Asia-Australia). Additionally, the fractal dimensions of forest cover are similar for all three continents with values of approximately 1.9 (Tab. 1). To analyse the shape of fragments we determined the fragment perimeter distributions and again, found for all three continents power law behaviour with similar exponents close to 2.2 (Tab. 1, Extended Data Fig. 1). Our results raise the question why varying patterns of local deforestation produce such remarkably similar fragmentation patterns at the continental scale.

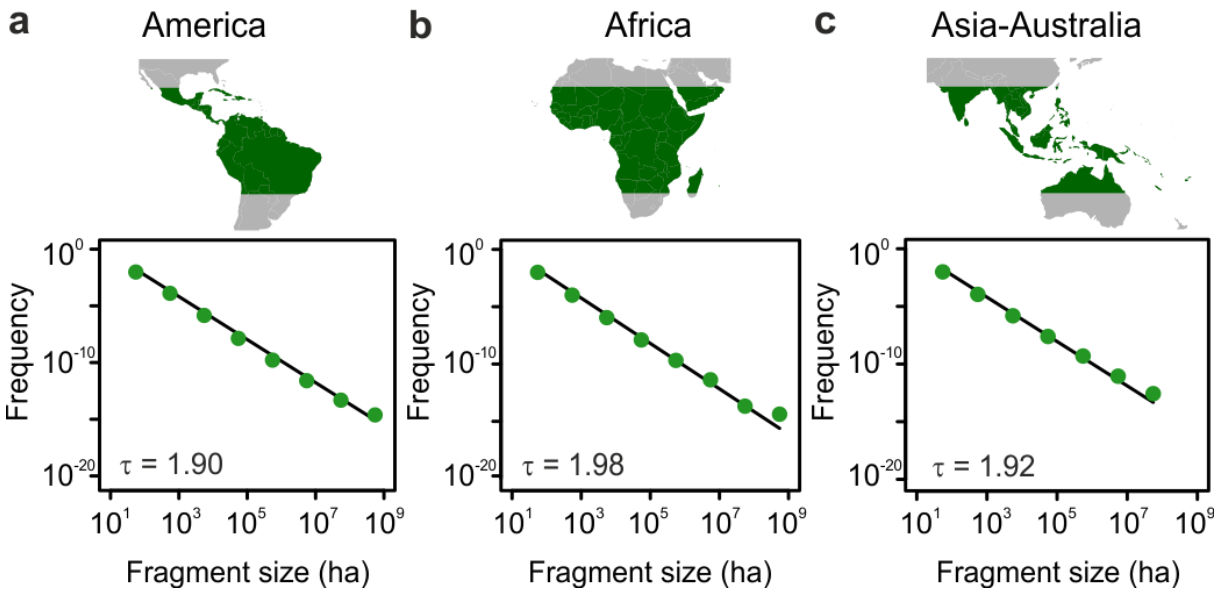

Figure 1: Continental-scale fragment size distribution of tropical and sub-tropical forests. Observed fragment size distribution (green dots, fragment sizes ≥ 10 ha) for **a**, America (n = 55.5 million fragments), **b**, Africa (n = 44.8 million fragments) and **c**, Asia-Australia (n = 30.5 million fragments), and fit of a power law distribution with exponent τ (solid line). The world map shows the selected tropical regions in green. Fragment sizes were estimated from Hansen's vegetation cover map[2].

Percolation theory[10,11] provides one possible explanation for the observed patterns. To briefly introduce the theory, imagine the cells of a landscape to be occupied with probability p by forest. Occupied cells, that share at least one side of a cell, form a forest fragment (also called 'cluster'). If p is large, the landscape is dominated by one large fragment spanning across the whole area (Extended Data Fig. 2a). However, for lower probabilities p the forest landscape is divided into smaller fragments, but still one large fragment exists that connects one side of the landscape with the other (the 'spanning cluster'). Note that the spanning cluster can show complex shapes with larger holes[11] (Extended Data Fig. 2b). When the probability p drops to a certain level ($p \approx p_c = 0.59$, equal to 59% forest area for large landscapes), the spanning cluster dissects and larger fragments disappear (Extended Data Fig. 2c, d).

The phases of fragmentation below and above a forest cover of 59% are defined as subcritical and supercritical, respectively, while the value of $p_c = 0.59$ itself represents the critical point of percolation where the large-scale behaviour of the system can be described by simple mathematical relationships[11,17]. For example, percolation theory predicts that the size distribution of fragments can be described by a power law with an exponent of $\tau \approx 2.05$ at the critical point (for infinite landscapes[10,11]). Interestingly, the empirical exponents of the forest cover map agree with the theory (τ between 1.9 and 2.0, Tab. 1). At the critical point, the

exponent of the fragment size distribution τ is further related to the fractal dimension d_f (via the hyperscaling relationship[11,18,19] $\tau = 1 + 2/d_f$). Theory predicts a fractal dimension of d_f = 1.89 (at the critical point[11]) which is in agreement with d_f values determined for the high-resolution forest cover map (1.92 for America and 1.87 for Africa and Asia-Australia, Tab. 1). Additionally, the perimeter distributions show power laws in agreement with the theoretical exponent[20] of $\kappa \approx 2.14$ (Tab. 1). Such critical exponents are often finger-prints of a system's hidden dynamics[7,9,21].

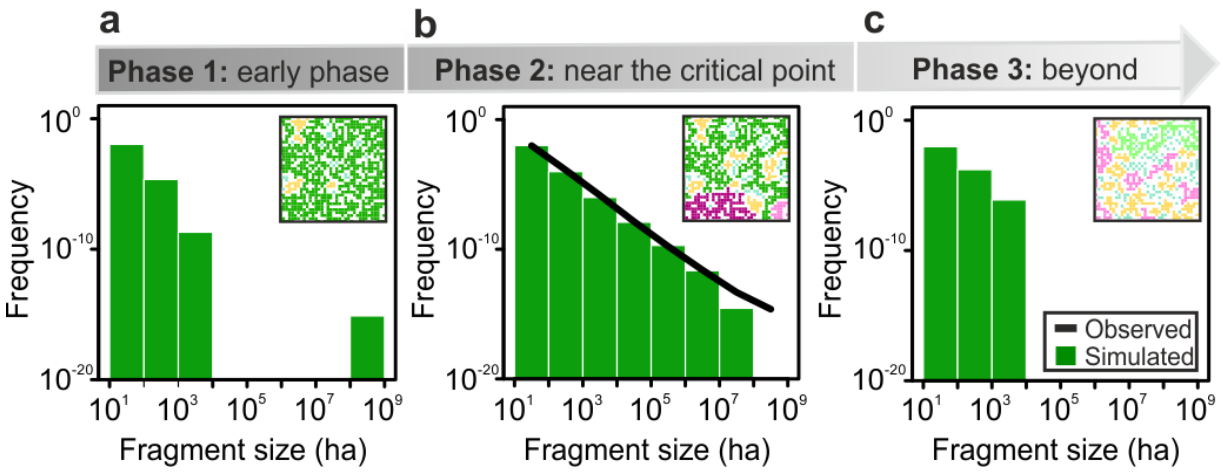

Figure 2: Dynamics of tropical forest fragmentation in America. Fragment size distributions (green bars: *FRAG* simulation, line: observation from remote sensing, fragment sizes ≥ 10 ha) and spatial patterns of fragments for different snapshots in time **a**, at the early phase, **b**, near the critical point of percolation and **c,** beyond. Shown is for each phase a map of a selected sub-area of 225 ha (*FRAG*, cleared sites are white and colours indicate different fragment sizes). Snapshots and a video are provided in Extended Data Fig. 3 and Supplementary Video 1.

Our empirical findings suggest that the observed tropical forest fragmentation is at all three continents near the critical point of percolation (reference year 2000). To test this hypothesis and to explore future dynamics, we developed and analysed three dynamic fragmentation models (*FRAG*, *FRAG-B*, *FRAG-P*). In *FRAG*, which corresponds to classical percolation theory[11], local forest sites are cleared randomly and independently each year[22,23] (Fig. 2, Extended Data Fig. 3, Supplementary Video 1). Deforestation happens across a landscape initially covered by forest. *FRAG-B* and *FRAG-P* were used to test our findings with respect to more complex deforestation and reforestation patterns as well as forest protection (see Methods for details). We analysed the dynamics of forest fragmentation for each continent and kept track of all forest fragments emerging during time. In total, approximately 3 Gha of forest area was simulated (33 billion cells of resolution 30 m × 30 m).

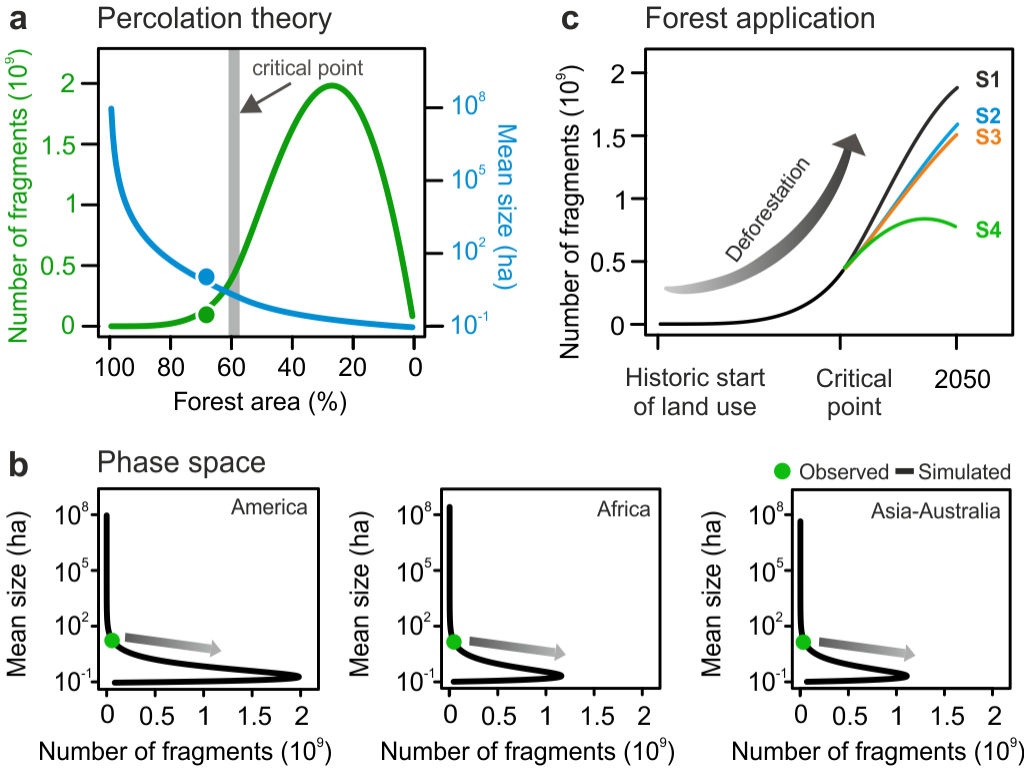

Figure 3: Percolation theory applied to observed forest fragmentation. a, Dynamics of the number of forest fragments (green line, linear scale) and mean fragment size (blue line, linear scale) with decreasing forest area (%) as observed by remote sensing (dots) and simulated by the fragmentation model *FRAG* (solid lines) for America. **b**, Number of fragments and their mean size show nonlinear behaviour for all three continents (solid lines: *FRAG* simulations, dots: observations from remote sensing). **c,** Application of percolation theory to project future forest fragmentation for different scenarios in America using *FRAG* (see Methods for details of scenarios *S1–S4*).

The dynamics of forest fragmentation as simulated by the *FRAG* model predict the empirically observed fragment size distributions (Fig. 2b). Forest removal beyond the critical point revealed a hump-shaped development of the numbers of fragments[24] (Fig. 3a, b). Below the critical point the number of fragments is rising slowly but accelerates strongly afterwards (maximum of 2000 million fragments for tropical America, Fig. 3a). The currently observed number of fragments and their mean size also matches those predicted by the *FRAG* model near the critical point (Fig. 3a, b). Though, small additional amounts of forest loss in the near future would lead to a strong increase in the number of forest fragments. We obtain similar trends for Africa and Asia-Australia (Fig. 3b).

We used the *FRAG* model to explore how forest fragmentation would proceed in the next decades based on our suggested explanation for the observed fragmentation patterns. Under

constant deforestation (0.51% per year in America[1] without any reforestation), the number of forest fragments will explode (maximum by factor 33 over 50 years, scenario *S1* in Fig. 3c, Extended Data Fig. 4a, e) while mean fragments' sizes decrease (from 17 ha to 0.25 ha in scenario *S1*, Fig. 3a, Extended Data Fig. 4a, e). To assess how reduced deforestation and reforestation may mitigate these effects, we analysed additional scenarios (Fig. 3c, Extended Data Fig. 4b–e). For example, considering reforestation (0.14% per year in America[1]) reduces the deforestation rate only slightly and still would lead to an increase of fragment number by factor 28 until 2050 (scenario *S2* in Fig. 3c). The same would arise for a yearly reduction in deforestation rate (derived from ref. 2) where the projected increase of fragment number is limited to factor 27 until 2050 (scenario *S3* in Fig. 3c). Only efforts that increasingly reduce deforestation rates in combination with reforestation (e.g., by 0.01%/year[2]) would lead to rising forest cover and decreasing fragment numbers after 20 to 30 years (scenario *S4* in Fig. 3c). Such mitigation scenarios are important aspects for an assessment of forest fragmentation. While Europe, North America and parts of Asia experienced higher reforestation than deforestation during the last centuries[25,26], forest loss still exceeds forest gain in most tropical countries[2,26] like Brazil, Indonesia and Cameroon.

Trends in both – increasing fragment numbers and decreases in their size – have important consequences for species habitats[3,27,28] and forest fragment edges[16,27] (Extended Data Fig. 4). They negatively impact biodiversity[16,27] by reducing fragments' connectivity and by enhancing edge effects. In addition, recent studies outlined that elevated tree mortality[16] in the edge area of forest fragments will lead to additional carbon emissions[29]. Effective policies and regulations for preventing negative effects of fragmentation thus require robust indicators. The development of indicators is an important challenge of environmental science, especially given the possibility that critical transitions of global ecosystems may occur due to human land transformations[30].

To test our results with respect to more complex spatial regimes of deforestation (*FRAG-B* model), we simulated deforestation to occur with probability d_{border} at the border of already existing forest fragments and at random locations otherwise (Extended Data Fig. 5, Supplementary Video 2). In terms of criticality, the *FRAG-B* model showed similar behaviour as the classical percolation model (*FRAG*) – for nearly the entire range of the parameter d_{border} (critical point at $p_c = 0.59$ with $\tau \approx 2$, Extended Data Fig. 6). In addition, border deforestation further widens the range of forest area where power law behaviour with exponent $\tau \approx 2$ occurs

(Extended Data Fig. 7). Reforestation (e.g., 0.14% per year in America[1]) is already well captured by our *FRAG* and *FRAG-B* models by lowering deforestation rates (Extended Data Fig. 8). Similarly, protection of forest (*FRAG-P* model) proportionally reduces the forest area that is prone to deforestation where the *FRAG* model still applies (simulated number of fragments scale with landscape size, Extended Data Figs. 9, 10). Although local landscape structures may differ due to local deforestation regimes, we found that the behaviour of the extended models collapses after suitable transformation in good approximation to that of the classical percolation model (*FRAG*). Reforestation and protecting large forest areas have nevertheless potentials to mitigate consequences of fragmentation (Extended Data Figs. 4, 10).

Our findings of the extended percolation models underpin the universality of fragmentation patterns close to the critical point. This is a general feature of critical phenomena: their large-scale behaviour is independent of the underlying small-scale mechanisms[7,17,21]. Even though land use appears to be complex and diverse, our outcomes emphasize simple mechanisms to be sufficient for describing forest fragmentation structures at larger scales. This finding does not exclude the possibility that the empirical patterns detected here may have alternative explanations. Our combination of spatial analyses of a high-resolution forest cover map, simulation modelling and application of percolation theory provides a first step towards a simple explanation for the intriguing global patterns of tropical forest fragmentation.

References

1 Achard, F. *et al.* Determination of tropical deforestation rates and related carbon losses from 1990 to 2010. *Global Change Biol* **20(8)**, 2540-2554 (2014).

2 Hansen, M. C. *et al.* High-resolution global maps of 21st-century forest cover change. *Science* **342(6160)**, 850-853 (2013).

3 Haddad, N. M. *et al.* Habitat fragmentation and its lasting impact on Earth's ecosystems. *Sci Adv* **1(2)**, e1500052 (2015).

4 Chaplin-Kramer, R. *et al.* Degradation in carbon stocks near tropical forest edges. *Nat Commun* **6**, 10158 (2015).

5 Storch, D., Marquet, P. A. & Brown, J. H. *Scaling Biodiversity*. (Cambridge University Press, 2007).

6 Marquet, P. A. *et al.* Scaling and power-laws in ecological systems. *J Exp Biol* **208(9)**, 1749-1769 (2005).

7 Sornette, D. *Critical Phenomena in Natural Sciences. Chaos, Fractals, Selforganization and Disorder: Concepts and Tools*. (Springer, 2006).

8 Turcotte, D. L. & Malamud, B. D. Landslides, forest fires, and earthquakes: examples of self-organized critical behavior. *Physica A* **340(4)**, 580-589 (2004).

9 Bak, P. *How Nature Works. The Science of Self-Organized Criticality*. (New York: Copernicus, 1996).

10 Stauffer, D. & Aharony, A. *Introduction to Percolation Theory*. (Taylor & Francis,

1994).
11 Christensen, K. & Moloney, N. R. *Complexity and Criticality*. Vol. 1 (Imperial College Press, 2005).
12 Le Quéré, C. *et al.* Global carbon budget 2014. *Earth Syst Sci Data* **7(1)**, 47-85 (2015).
13 Wright, S. J. Tropical forests in a changing environment. *Trends Ecol Evol* **20(10)**, 553-560 (2005).
14 Lewis, S. L., Edwards, D. P. & Galbraith, D. Increasing human dominance of tropical forests. *Science* **349(6250)**, 827-832 (2015).
15 Houghton, R. A. The worldwide extent of land-use change. *Bioscience* **44(5)**, 305-313 (1994).
16 Laurance, W. F. *et al.* The fate of Amazonian forest fragments: A 32-year investigation. *Biol Conserv* **144(1)**, 56-67 (2011).
17 Saberi, A. A. Recent advances in percolation theory and its applications. *Phys Rep* **578**, 1-32 (2015).
18 Milne, B. T. *et al*. Detection of critical densities associated with piñon-juniper woodland ecotones. *Ecology* **77(3)**, 805-821 (1996).
19 Drossel, B. & Schwabl, F. Self-organized critical forest-fire model. *Phys Rev Lett* **69(11)**, 1629 (1992).
20 Ziff, R. M. Test of scaling exponents for percolation-cluster perimeters. *Phys Rev Lett* **56(6)**, 545 (1986).
21 Solé, R. V. & Bascompte, J. *Self-Organization in Complex Ecosystems*. Vol. 42 (Princeton University Press, 2006).
22 Turner, M. G., Gardner, R. H. & O'Neill, R. V. *Landscape Ecology in Theory and Practice*. (New York: Springer, 2001).
23 Gardner, R. H., Milne, B. T., Turner, M. G. & O'Neill, R. V. Neutral models for the analysis of broadscale landscape pattern. *Landscape Ecol* **1(1)**, 19-28 (1987).
24 Bascompte, J. & Solé, R. V. Habitat fragmentation and extinction thresholds in spatially explicit models. *J Anim Ecol* **65(4)**, 465-473 (1996).
25 Meyfroidt, P. & Lambin, E. F. Global forest transition: prospects for an end to deforestation. *Annu Rev Env Resour* **36**, 343-371 (2011).
26 Rudel, T. K. *et al*. Forest transitions: towards a global understanding of land use change. *Global Environ Chang* **15(1)**, 23-31 (2005).
27 Debinski, D. M. & Holt, R. D. A survey and overview of habitat fragmentation experiments. *Conserv Biol* **14(2)**, 342-355 (2000).
28 Andrén, H. Effects of habitat fragmentation on birds and mammals in landscapes with different proportions of suitable habitat: a review. *Oikos* **71(3)**, 355-366 (1994).
29 Brinck, K. *et al.* High resolution analysis of tropical forest fragmentation and its impact on the global carbon cycle. *Nat Commun* **8**, 14855 (2017).
30 Barnosky, A. D. *et al.* Approaching a state shift in Earth's biosphere. *Nature* **486(7401)**, 52-58 (2012).

Supplementary Information is linked to the online version of the paper at www.nature.com/nature.

Acknowledgments

The project has been supported by the Helmholtz Allianz Remote Sensing and Earth System Dynamics. A.H. and T.W. were supported by the ERC advanced grant 233066. We thank

Anne Hein and André Bogdanowski for assistance, Alexander K. Hartmann for discussion, Mateus Dantas de Paula for data handling, Sebastian Paulick and Friedrich Bohn for technical support.

Author contributions

A.H., F.T. and R.F. conceived the project. A.H., F.T. and T.W. supervised the research. S.L. and E.R. processed and analysed vegetation maps. F.T. performed statistical analysis of map observations. F.T. and M.M. implemented the simulation models and conducted the simulations. F.T. analysed the results and prepared figures, tables and videos. A.H., F.T., R.F., T.W. and J.G. wrote the manuscript. All authors have participated in discussion and editing of the manuscript.

Author information

The authors declare no competing financial interests.

Correspondence and requests for materials should be addressed to franziska.taubert@ufz.de.

Methods

Used forest cover map and its analysis

The analysis of global forest fragmentation is based on Hansen's forest cover map[2] that uses Landsat observation for year 2000 with a spatial resolution of 30 m × 30 m. We used a forest/non-forest classification threshold of 30% (minimum forest cover per pixel) in this study.

The resulting image shows non-forested and forested pixels (original binary image files were processed as in ref. 29, ascii format, WGS-84 projection), whose connection to forest fragments is determined by its 4-pixel neighbourhood (open boundary conditions). For this, an extended cluster detection algorithm was used[29]. The area of a pixel in the WGS-84 projection is calculated dependent on its geographical position[29]. As area calculation for every pixel is highly time consuming (224 billion pixels for land surface in the tropics), we pre-calculated the area size of pixels along 256 latitudes.

Please note that maps in Fig. 1 show the entire land area of the tropical belt. Maps were

created using R (ref. 31) and the package 'rworldmap' (ref. 32).

Forest fragmentation model *FRAG*

For simulation of fragmentation dynamics we used a landscape with C_{max} cells of size s (30 m × 30 m). Cells can have two states (forested or deforested). We start the simulation with a fully forested area (all cells are in 'forest' state, total forest area is $A_{max} = C_{max}\, s$). In each step (here, one year) some forest area is cleared assuming a constant deforestation rate d (% per year). That means, a certain number of forest cells ($C_{max}\, d$) is randomly selected and assigned to the state 'deforested' in each year.

For simplicity, cells do not regenerate back to forest in the *FRAG* model, so forest area is successively reduced within time until the entire forest area is cleared. However, deforestation rates used in *FRAG* can also be interpreted as net deforestation rates that result from reforestation and gross deforestation occurring at random sites. In detail, with d being the yearly gross deforestation rate (e.g., 0.51% per year derived from ref. 1 for tropical America) and r being the yearly reforestation rate (e.g., 0.14% per year derived from ref. 1 for tropical America), we obtained a yearly net deforestation rate of $d_{net} = d - r$. Including random reforestation into our simulations thus shows that the effect of reforestation is already covered by the *FRAG* model (Extended Data Fig. 8a). If reforestation occurs exclusively at the border of forest fragments, small deviations can be observed (median deviations show 5% lower fragment numbers than for random reforestation).

We analysed results of the fragmentation model using the same methods as for the analysis of the high-resolution forest cover map in terms of remaining forest area, fragment numbers and their mean size as well as the fragment size distribution (see 'Analysis and statistics of tropical forest fragmentation'). Dynamics of fragment numbers scale with landscape size C_{max} (total number of cells, Extended Data Fig. 9a). Normalized fragment numbers can thus be calculated by dividing the absolute number of fragments by the total number of cells (C_{max}).
The critical point p_c is determined as the remaining forest area relative to landscape area A_{max} after which the spanning cluster no longer exists. The spanning cluster is defined as any large cluster which expands from one border of the landscape to an opposite side border (either north to south or east to west). Note that this simple fragmentation model corresponds to a dynamic version of the classical percolation model[10,11,22,23].

Simulation of forest fragmentation at the continental scale

Potential forest areas before forest clearing have been estimated for each continent using a map of vegetation biomes[33] selecting for classified tropical forest area (only biomes of tropical and sub-tropical woodland). Potential areas have been calculated by remapping vegetation cover of gridded maps (0.5° × 0.5°) to an equidistant map (1 km × 1 km) using climate data operators (*cdo*)[34].

We simulated forest fragmentation dynamics by using for each continent the estimated potential forest cover (used cell size s = 30 m × 30 m) and deforestation rates derived from literature (Tab. 1). Extents of simulated continental areas for the fragmentation model were 1,377 million ha for America, 806 million ha for Africa and 770 million ha for Asia-Australia (corresponding to C_{max} of 15,300,205,636 cells for America, 8,955,555,556 cells for Africa and 8,555,555,556 cells for Asia-Australia). To determine the current forest area (in %) in Fig. 3a, we divided the observed forest areas (from remote sensing, Tab. 1) by the estimated potential forest areas. Gross deforestation rates (Tab. 1) and reforestation rates were derived from ref. 1 by dividing area change estimates of annual gross deforestation (2000-2010) and annual forest regrowth (2000-2010) by area estimates of forest cover (2000) for dry and humid tropical forests. Please note that potential forest area estimates can include uncertainties which can affect the determined fraction of current forest area (in %) for the forest cover map.

Simulation scenarios of future forest fragmentation patterns

We simulated four different scenarios (*S1* to *S4*) to project future development of forest fragmentation (until 2050 for America, using *FRAG*, Extended Data Fig. 4):

Scenario S1: Net deforestation rate is constant at d_{net} = 0.51% per year (ref. 1). This scenario assumes no reforestation.

Scenario S2: Deforestation of d = 0.51% per year (ref. 1) is counterbalanced by reforestation of r = 0.14% per year (ref. 1). This results in an effective net deforestation rate of d_{net} = 0.37% per year.

Scenario S3: Deforestation rate of 0.37% per year (ref. 1) is reduced each year by

0.0012%/year^2. This results in a net deforestation rate of $d_{net} = a - bt$, with t being years passed since the critical point, a = 0.37% per year and b = 0.0012%/year^2. This scenario for tropical America was based on a 12-year observation of forest gain and forest loss (ref. 2, version v1.3). Derived absolute values of net forest area change were related to our simulated landscape area (A_{max}) and fitted by linear regression (slope = 0.0012, R^2 = 0.013).

Scenario S4: Deforestation of 0.37% per year (ref. 1) is reduced each year by 0.01%/year^2. This results in a net deforestation rate of $d_{net} = a - bt$ (with a = 0.37% per year and b = 0.01%/year^2) with a turning point at which forest recovery exceeds deforestation. This scenario is similar to *S3*, but with a stronger decreasing trend of yearly deforestation rates.

Projections of future fragmentation for year 2050 started from the critical point of percolation using the *FRAG* model (as a simplification). A time step corresponds to a constant reduction of forest area per year. Projected values (of fragment numbers and mean size in 2050) for different deforestation scenarios (Fig. 3c) were compared to observational values from remote sensing (Tab. 1, factors shown in Extended Data Fig. 4). The fragmentation dynamics (in terms of deforestation rate, forest cover, fragment numbers and mean fragment size) for each scenario are shown in Extended Data Fig. 4 (absolute values can be found in Extended Data Fig. 4e).

Forest fragmentation model *FRAG-B*

In addition, we analysed a second version of the fragmentation model in order to test for more complex deforestation patterns. To this end, a probability d_{border} to clear only forested cells at the border of a forest fragment has been introduced. When d_{border} = 0, forested cells are cleared randomly (*FRAG* model version). When d_{border} = 0.5, 50% of the deforestation is restricted to fragment borders while the remaining 50% is still deforested all over the place. When d_{border} = 1, only cells at the border of forest fragments are cleared (with random site selection for deforestation in the first time step). We analysed the result of the *FRAG-B* model similar to *FRAG* (see 'Analysis and statistics of tropical forest fragmentation'). Dynamics of fragment number also scale with landscape size C_{max} (Extended Data Fig. 9b). Thus, normalized fragment numbers can again be calculated by dividing the absolute number of fragments by the total number of cells (C_{max}).

Gross deforestation rates used in the *FRAG-B* model can again be interpreted as net

deforestation rates that result from reforestation at random sites together with border gross deforestation (similar to *FRAG*, Extended Data Fig. 8b). In this case, the probability, that deforestation occurs at the border of forest fragments (d_{border}), changes to approximately $d_{border,net} = (d_{border}\ d - r)/(d - r)$, with d being the yearly gross deforestation rate (e.g., 0.51% per year in America[1]) and r being the yearly reforestation rate (e.g., 0.14% per year in America[1]). Small deviations can be attributed to the dynamic change of border area of fragments during the simulation. In contrast, reforestation is fully captured by our *FRAG-B* model if reforestation occurs with the same probability d_{border} at the border of forest fragments as deforestation does.

In order to test for a full range of border deforestation, we simulated a forest landscape ($C_{max} = 10^6$ cells) and varied d_{border} from 0 to 1 in steps of 0.1. Between $d_{border} = 0.9$ and $d_{border} = 1.0$ we tested model behaviour for detailed values: $d_{border} = 0.925$, 0.95, 0.975, 0.98, 0.985, 0.99, and 0.995 (because critical points and power law exponents of fragment sizes drop between $d_{border} = 0.9$ and $d_{border} = 1.0$). We focused our analysis on the critical points and the fitted power law exponents of fragment size distributions for each simulation (Extended Data Fig. 6) with the following sample sizes of fragments: $n = 29{,}788$ ($d_{border} = 0$), $n = 30{,}195$ ($d_{border} = 0.1$), $n = 29{,}020$ ($d_{border} = 0.2$), $n = 28{,}131$ ($d_{border} = 0.3$), $n = 31{,}117$ ($d_{border} = 0.4$), $n = 30{,}506$ ($d_{border} = 0.5$), $n = 30{,}733$ ($d_{border} = 0.6$), $n = 34{,}182$ ($d_{border} = 0.7$), $n = 35{,}325$ ($d_{border} = 0.8$), $n = 43{,}045$ ($d_{border} = 0.9$), $n = 44{,}997$ ($d_{border} = 0.925$), $n = 45{,}964$ ($d_{border} = 0.95$), $n = 45{,}577$ ($d_{border} = 0.975$), $n = 44{,}415$ ($d_{border} = 0.98$), $n = 45{,}692$ ($d_{border} = 0.985$), $n = 43{,}806$ ($d_{border} = 0.99$), $n = 38{,}875$ ($d_{border} = 0.995$), $n = 1{,}278$ ($d_{border} = 1.0$) fragments.

Forest fragmentation model *FRAG-P*

A third version of the fragmentation model includes protected forest areas. To this end, a fraction $f_{protected}$ of landscape area (in total $f_{protected}\ A_{max}$) is preserved against deforestation. When $f_{protected} = 0$, forest area is cleared randomly (*FRAG* model). When $f_{protected} = 0.5$, 50% of forest area is protected while the remaining 50% are still deforested randomly. When $f_{protected} = 1$, no forest area will be cleared. The protected forest area is distributed among rectangular forest patches (of 10,000 ha in size) that are randomly distributed across the landscape. In order to reach the total protected area exactly ($f_{protected}\ A_{max}$), also a few forest patches of different size are allowed for protection (e.g., if protected forest patches overlap or are placed too close to the landscape boundaries).

Conceptually, protecting large forest fragments means preserving certain size classes in the fragment size distribution (e.g., in our *FRAG-P* model the size class $[10^4; 10^5)$ ha). Thus, protection of one large fragment is equivalent to excluding this fragment from the study area which is prone to deforestation (e.g., similar to *FRAG*). Because the normalized number of fragments (normalization means dividing by the total number of cells C_{max}) is independent of landscape size, we obtain a behaviour that is captured by *FRAG* also for smaller landscape areas (Extended Data Fig. 9). This property reduces the extrapolated number of forest fragments proportionally by $(1 - f_{protected})$ (Extended Data Fig. 10).

In order to test for a range of protected forest area, we simulated different fractions of protected areas ($f_{protected}$ = 0.1 and 0.5, for landscape sizes compared to tropical America, i.e. C_{max} = 15,300,205,636 cells). We focused our analysis on the number of forest fragments (Extended Data Fig. 10).

Analysis and statistics of tropical forest fragmentation

Forest fragments have been detected by applying an extended cluster detection algorithm[29]. This algorithm labels each single fragment of cells based on the direct four neighbours per cell (see section 'Used forest cover map and its analysis'). The mean fragment size of a landscape is calculated by summing up their sizes divided by the number of fragments (unweighted mean including the spanning cluster).

We calculated the fragment size distribution, i.e. the number of fragments per fragment size class. In order to describe its form, we applied multinomial maximum likelihood estimation of logarithmically binned data to fragment sizes published by Virkar and Clauset[35] (using the *Matlab* package provided online). We fitted the frequency of fragment sizes to a power law distribution to determine the scaling exponent ($N(f) \sim f^{-\tau}$ with $N(f)$ as the number of fragments of size f and τ as the scaling exponent). For logarithmic binning, we used size classes $[10^1; 10^2)$, $[10^2; 10^3)$ … $[10^8; 10^9)$ in ha. We excluded fragments smaller than 10 ha for the fit. Standard errors[35] for each fitted exponent were calculated by bootstrapping (1,000 repetitions). Goodness of fit was evaluated by using Pearson's correlation coefficient (R) between predicted and empirical cumulative distributions (both logarithmic; using raw data including also empirical and simulated fragments smaller than 10 ha). Similar to fragment sizes, we calculated perimeters (edge length) of detected forest fragments for analysing and fitting the fragment perimeter distribution ($N(l) \sim l^{-\kappa}$ with $N(l)$ being the frequency of

fragments with perimeter l and κ being the scaling exponent). For logarithmic binning, we used perimeter classes [10^3; 10^4), [10^4; 10^5) … [10^9; 10^{10}) in m and excluded fragment perimeters smaller than 1,000 m for the fit (equivalent to approximately 10 ha of fragment size). Standard errors[35] were again derived for each fitted exponent by bootstrapping (1,000 repetitions). Goodness of fit was similarly evaluated by using Pearson's correlation coefficient (R) between predicted and empirical cumulative distributions (both logarithmic; using raw data including also empirical and simulated fragment perimeter smaller than 1,000 m).

We further determined the fractal dimension d_f based on subsequently grouping 30 m × 30 m cells of the vegetation map to boxes of $b_f = 2^1, 2^2, 2^3, \ldots, 2^8$ cells (box counting method[36,37]). For each box we determined how many cells include forest. When at least one cell per box is occupied by forest, we mark the entire box as forested. By this, a map of coarser resolution than the original map (with s = 30 m × 30 m resolution) is created. The fractal dimension is then calculated by relating the inverse of b_f to the number of boxes including forest on the landscape of coarser resolution. This relationship follows a power law whose scaling exponent represents the fractal dimension. We fitted this relationship on log-log axes by using ordinary least squares regression and calculated the corresponding coefficient of determination R^2. We calculated the fractal dimension d_f for the high-resolution vegetation map (Tab. 1, with R^2 values of approximately 1 for each continent) and compared them to the predicted dimension $d_f = 1.89$ of percolation theory[11]. Note that deviations in the exponent τ of the fragment size distribution trace back to the finite area of the continents while the calculation of fractal dimension is not affected by the finite area.

The large extent of our simulated forest landscapes retains variations of results for replicate simulations low. We calculated the coefficient of variation (standard deviation σ divided by mean value μ, $CV = \sigma/\mu$) from 10 repeated simulations for each time step. Finally, we determined the median CV_{median} as an aggregated statistic for all time steps for the number and mean size of fragments. For the fragment size distribution, we only calculated the CV at the critical point for each class of fragment sizes and determined the median CV_{median} for all size classes (see above for details on size classes). For fragment number and mean size, median CV_{median} were below 0.00004 for all three continents (using *FRAG*, CV_{median} decreased in general during the simulation time). Median CV_{median} among size classes of the fragment size distribution (at the critical point) were less than 0.0062 (CV_{median} decreased in general with

smaller size classes). Similar results were obtained for *FRAG-B* (0.00004 and 0.0036 for d_{border} = 0.9, landscape area of America) and *FRAG-P* (0.00003 and 0.448 for $f_{\text{protected}}$ = 0.1, landscape area of America). Because stochasticity did not translate into visible effects, we visualized only one simulation run in Fig. 2, Fig. 3 and Extended Data Figs. 3–10 and provided absolute values of one simulation run in Extended Data Fig. 4e.

Visualisation of fragmentation patterns

We gathered snapshots of fragment size distributions and spatial patterns for each simulated year in our *FRAG* and *FRAG-B* model for America in MPG-files (Supplementary Video 1, 2) and figures (Fig. 2, Extended Data Figs. 3, 5). For the fragment size distribution, green bars show the simulation results (*FRAG* or *FRAG-B*) and the black line shows the observed size distribution (from remote sensing) for the tropical forest in America. We used logarithmic binning of fragment size classes $[10^1; 10^2)$, $[10^2; 10^3)$ … $[10^9; 10^{10})$ in ha. For graphical purposes only, we additionally visualized size classes $[10^{-1}; 10^0)$ and $[10^0; 10^1)$. Remaining forest area is provided within the barplot of the videos. For the shown map (selected sub-area of 900 ha was used for Extended Data Figs. 3 and 5 as well as for Supplementary Video 1 and 2, selected sub-area of 225 ha was used for Fig. 2 for graphical purposes), each fragment is coloured according to its size. Six size classes were chosen with the following colour codes: size < 0.4 ha (light blue), 0.4 ha < size < 2 ha (yellow), 2 ha < size < 9 ha (light magenta), 9 ha < size < 42 ha (light green), 42 ha < size < 195 ha (dark magenta), size > 195 ha (dark green). White cells denote cleared sites.

Code availability

The extended cluster detection software and the simulation models are available upon request (corresponding author).

Data availability

Data of observed fragments size and perimeter distributions and of simulation studies are available upon request (corresponding author).

References of methods

31 R Core Team. R: A language and environment for statistical computing. R Foundation for Statistical Computing, Vienna, Austria (2015), https://www.R-project.org/.

32 South, A. rworldmap: A New R package for Mapping Global Data. *The R Journal* **3(1)**, 35-43 (2011).

33 Ostberg, S., Schaphoff, S., Lucht, W. & Gerten, D. Three centuries of dual pressure

from land use and climate change on the biosphere. *Environ Res Lett* **10(4)**, 044011 (2015).
34 CDO 2015: Climate Data Operators. The Max Planck Institute for Meteorology, http://www.mpimet.mpg.de/cdo (2017).
35 Virkar, Y. & Clauset, A. Power-law distributions in binned empirical data. *Ann Appl Stat* **8(1)**, 89-119 (2014).
36 Sugihara, G. & May, R. M. Applications of fractals in ecology. *Trends Ecol Evol* **5(3)**, 79-86 (1990).
37 Bisoi, A. K. & Mishra, J. On calculation of fractal dimension of images. *Pattern Recogn Lett* **22(6)**, 631-637 (2001).

Extended Data Figures

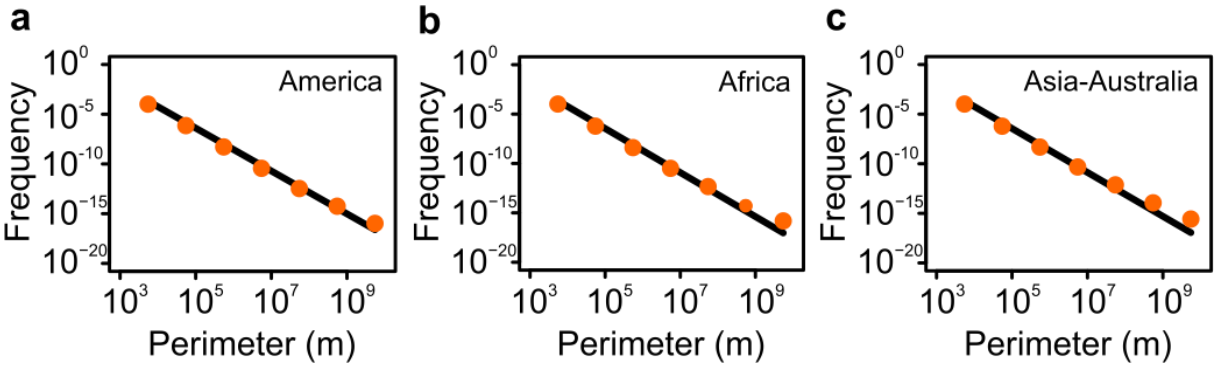

Extended Data Figure 1: Continental-scale fragment perimeter distribution of tropical and sub-tropical forest. Observed fragment perimeter distribution (orange dots; fragment perimeters > 1,000 m) for **a**, America (n = 55.5 million fragments), **b**, Africa (n = 44.8 million fragments) and **c**, Asia-Australia (n = 30.5 million fragments), and fitted power law with exponent κ (solid black line). Forest fragments were estimated from Hansen's forest cover map[2] (see Methods for details).

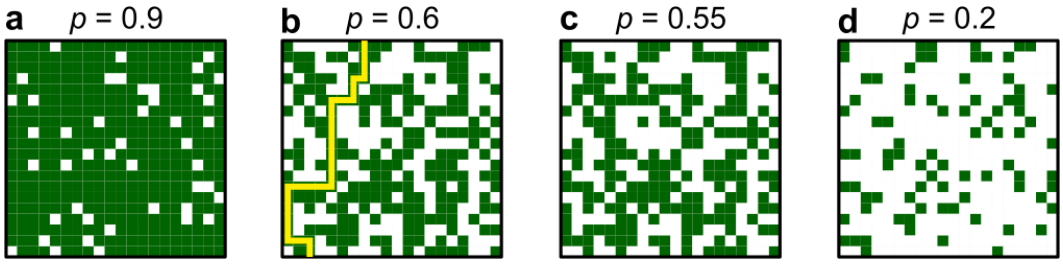

Extended Data Figure 2: Illustration of the concept of classical percolation theory. a, A landscape occupied by 90% randomly and independently distributed forest cells (green, p = 0.9) is dominated by one large cluster. **b**, For values of p larger than the percolation threshold (p = 0.6 > 0.59) a continuous path from two opposite side borders exists (yellow path within the spanning cluster). **c**, Below the percolation threshold (here, p = 0.55 < 0.59) larger clusters emerge but no spanning cluster can be detected. **d**, A landscape occupied by 20% forest shows small unconnected clusters. Landscape size is 20 × 20 cells.

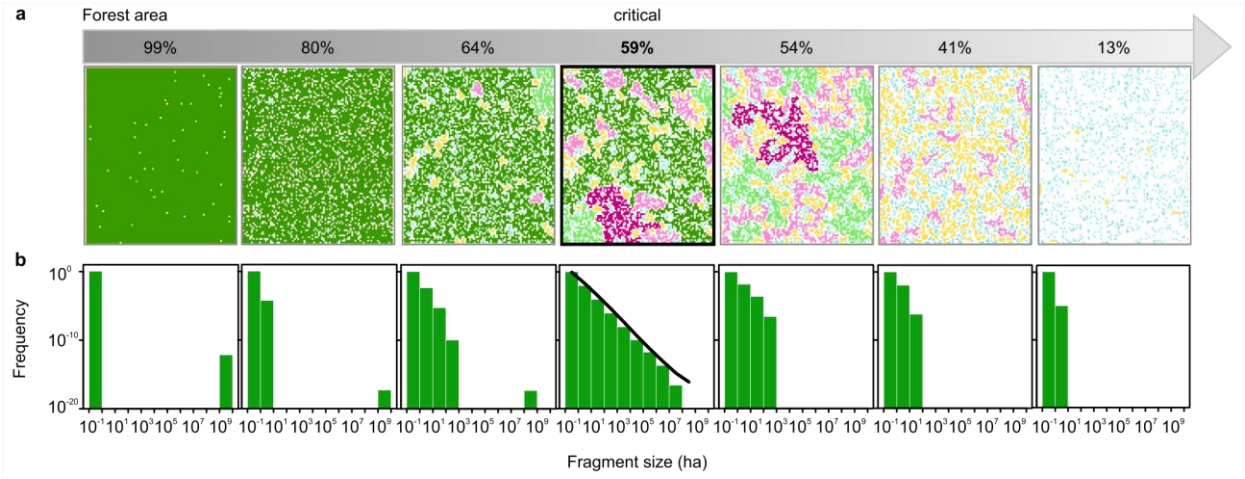

Extended Data Figure 3: Dynamics of tropical forest fragmentation in America using *FRAG*. **a**, Spatial patterns of fragments for different snapshots in time and **b**, fragment size distributions (green bars: *FRAG*, line: observation from remote sensing). The critical phase at which the spanning fragment disappears is indicated as 'critical'. For each phase a map of a selected sub-area of 900 ha is shown (*FRAG*, cleared sites are white and colours indicate fragment size, see Methods for details). For graphical purposes only, fragments < 10 ha are also shown. A video is provided (Supplementary Video 1).

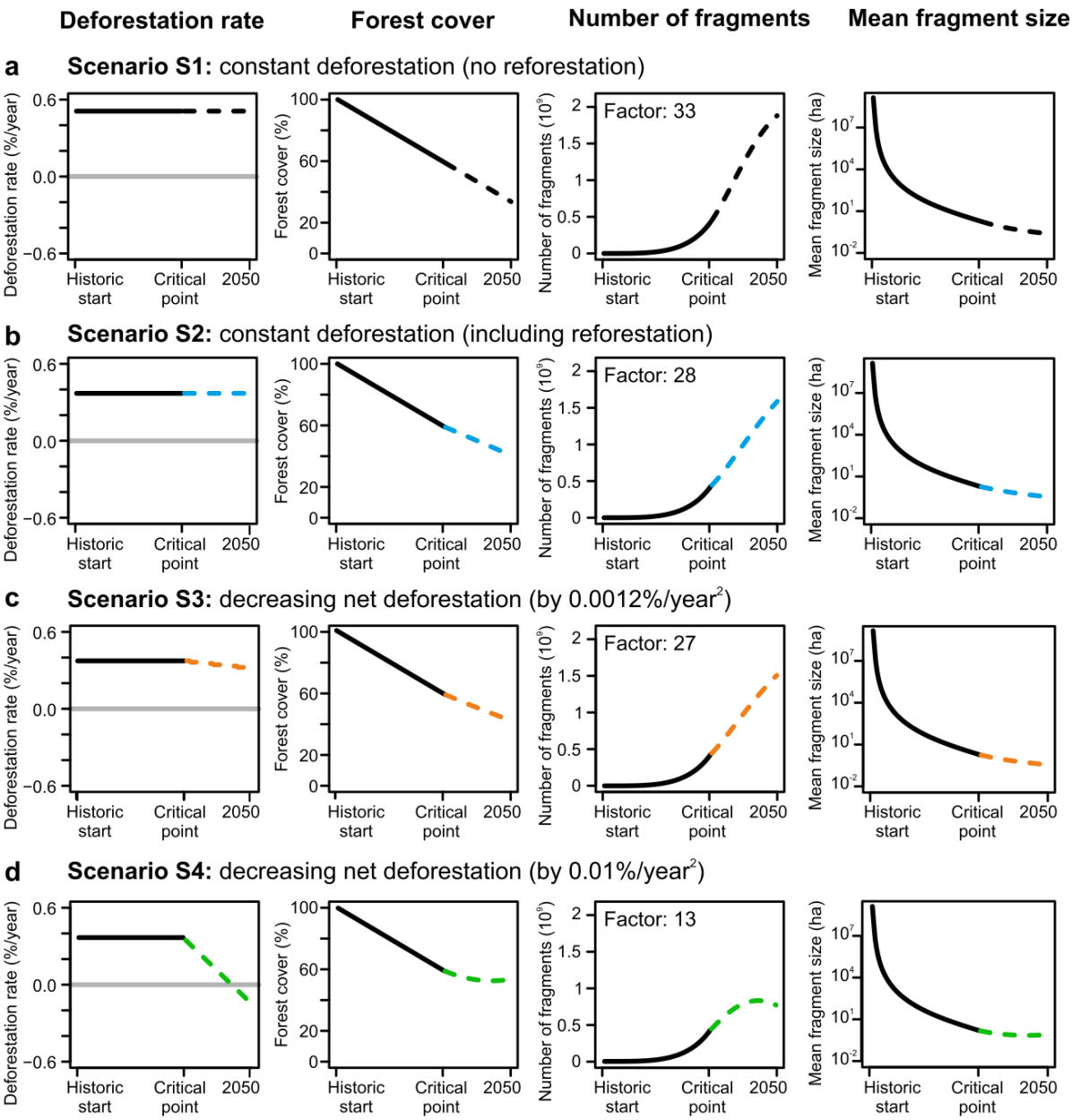

e Results of scenarios

	Observation*	Scenario S1†	Scenario S2†	Scenario S3†	Scenario S4†
Number of fragments (10^6)	55.5	1,880.4	1,587.4	1,507.2	772.1
Mean fragment size (ha)	17	0.25	0.35	0.39	0.95

* year 2000
† for year 2050

Extended Data Figure 4: Dynamics of fragmentation scenarios projected until 2050. Dynamics of deforestation rate (% per year related to landscape size), forest cover (%), number of fragments and mean fragment size (ha) in America projected until 2050 using *FRAG*. **a**, Scenario *S1* assumes constant deforestation without reforestation while **b**, scenario *S2* considers added reforestation. **c**, Scenario *S3* assumes a yearly increasing reduction of deforestation while **d**, in Scenario *S4* a stronger yearly reduction leads to a turning point with net reforestation. See Methods for details. **e**, Comparison of observed (Tab. 1) and projected fragment numbers (rounded) and mean fragment size.

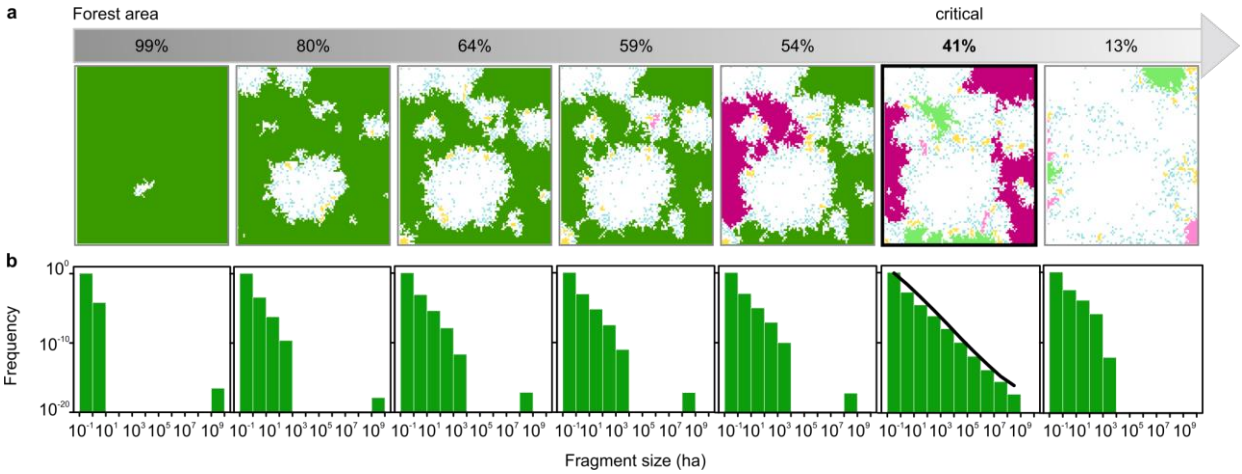

Extended Data Figure 5: Dynamics of tropical forest fragmentation in America using *FRAG-B*. **a**, Spatial patterns of fragments for different snapshots in time and **b**, fragment size distributions (green bars: *FRAG-B*, d_{border} = 0.995, line: observation from remote sensing). The critical phase at which the spanning fragment disappears is indicated as 'critical'. Shown is for each phase a map of a selected sub-area of 900 ha (*FRAG-B*, cleared sites are white and colours indicate fragment size, see Methods for details). For graphical purposes only, fragments < 10 ha are also shown. A video is provided (Supplementary Video 2).

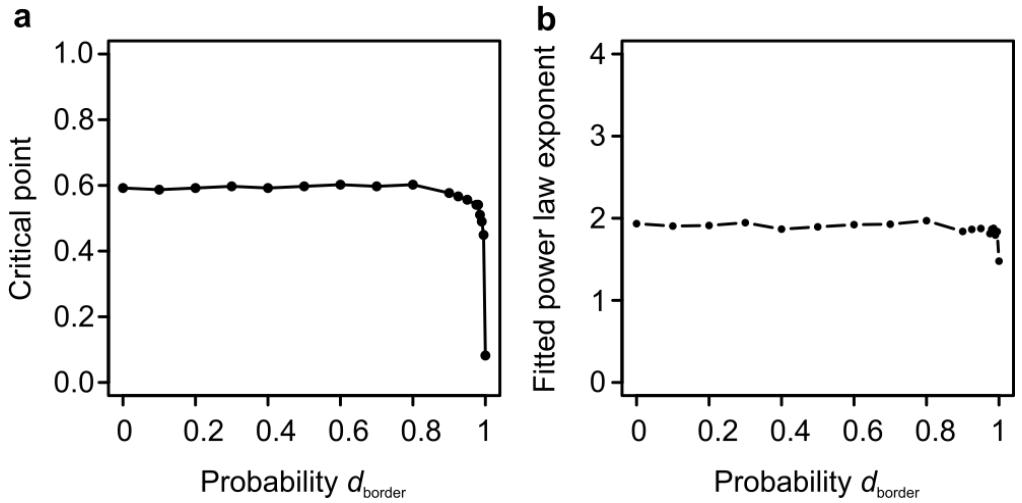

Extended Data Figure 6: The effect of border deforestation on fragmentation dynamics. **a**, Critical points and **b**, fitted power law exponents of fragment sizes for different probabilities (d_{border}) of deforestation restricted to the border of forest fragments (*FRAG-B* model for landscape size of $C_{max} = 10^6$ cells). Each point in **b**, represents one power law fit based on n = 29,788 (d_{border} = 0) to n = 1,278 (d_{border} = 1.0) fragments (see Methods for detailed values). Calculated R^2 values of fits are approximately 1 for the entire range of d_{border} probabilities (see Methods).

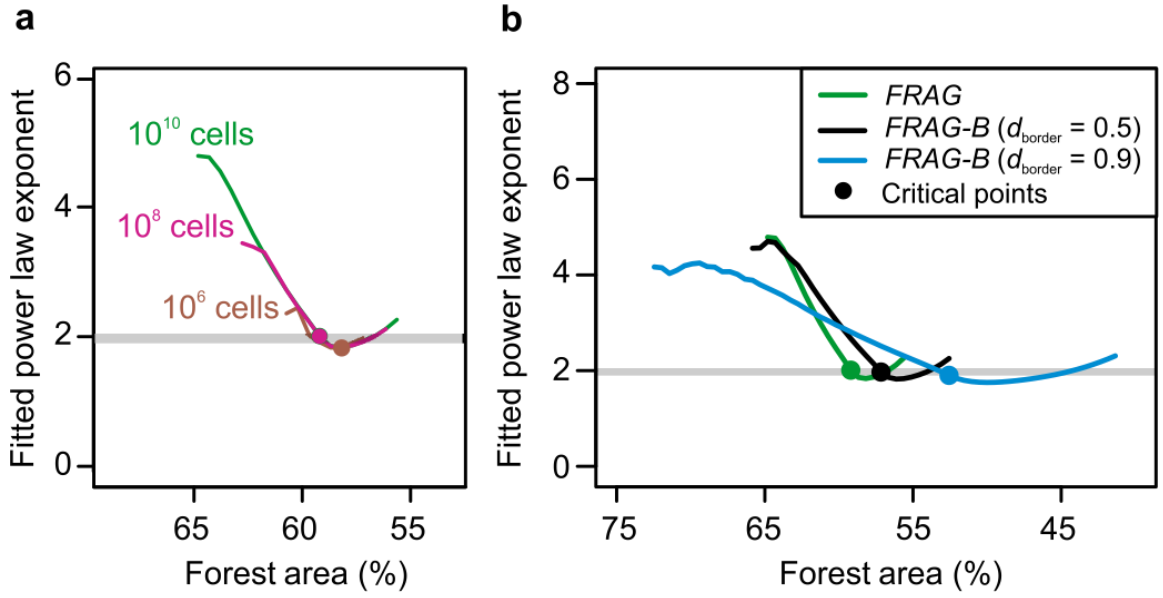

Extended Data Figure 7: Power law exponents fitted to simulated fragment size distributions. a, For different landscape sizes C_{max} based on the *FRAG* model and **b**, comparison between random (*FRAG*) and border deforestation (*FRAG-B*, d_{border} = 0.5 and d_{border} = 0.9). In **b**, landscape size was $C_{max} = 10^{10}$ cells. In both panels we show only results for fits with correlation coefficients $R^2 \geq 0.9$. The grey horizontal line shows the exponent predicted by percolation theory.

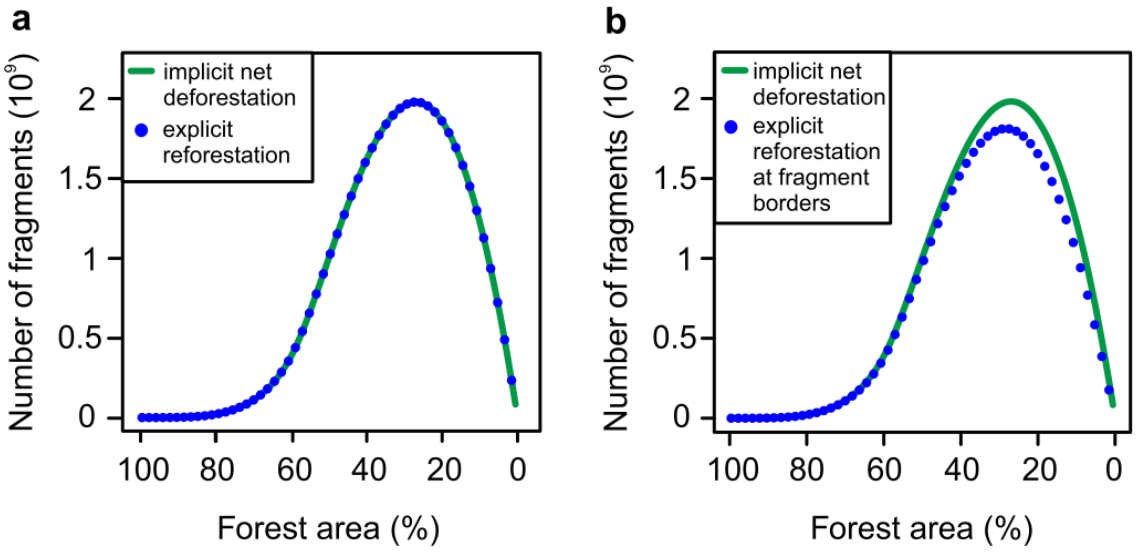

Extended Data Figure 8: Dynamics of fragment numbers comparing implicit and explicit modelling of reforestation. a, We assume a gross deforestation rate of d = 0.51% per year and a reforestation rate of r = 0.14% per year for America[1] (with random and independent selection of sites for deforestation and reforestation, blue dots). This model version is equivalent to the original *FRAG* model assuming a net deforestation rate of d_{net} = 0.37% per year (green line). **b**, The same scenario (green line as in **a**,) but now explicit reforestation exclusively occurs at the border of forest fragments (blue dots).

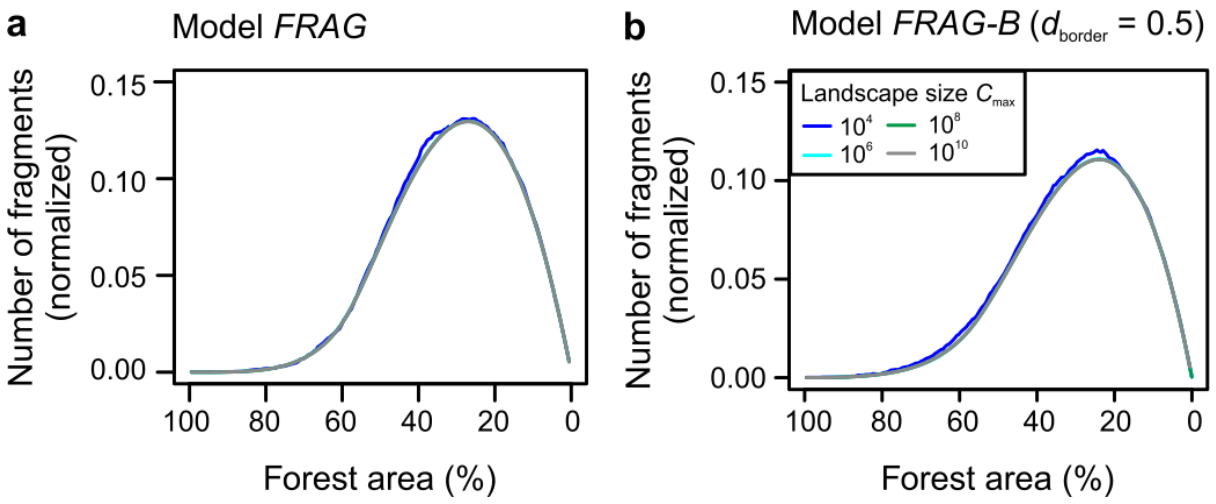

Extended Data Figure 9: Scaling of fragmentation dynamics. Dynamics of forest fragment numbers (normalized by landscape size C_{max}) in America using **a**, *FRAG* and **b**, *FRAG-B* (d_{border} = 0.5) for different landscape sizes. The pattern is independent of landscape size.

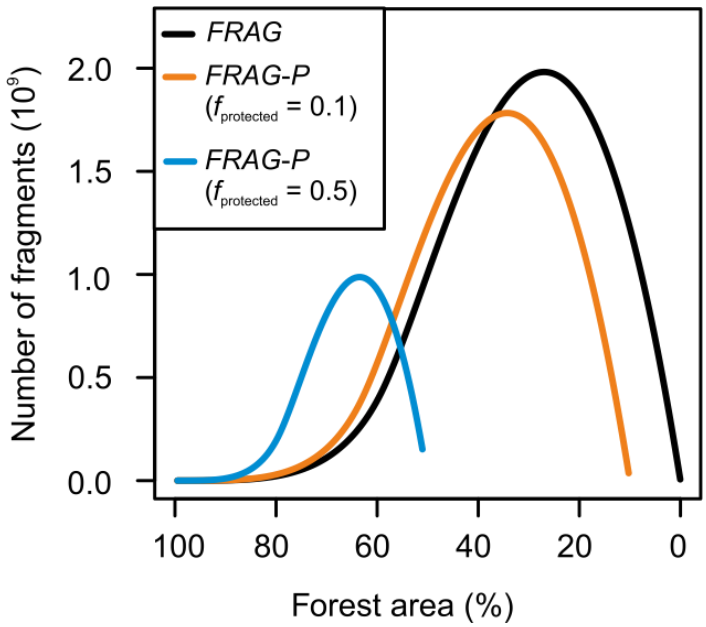

Extended Data Figure 10: Dynamics of the number of forest fragments without (*FRAG*) and with considering protected forest areas (*FRAG-P*). Simulations with the *FRAG-P* model account for 10% ($f_{protected}$ = 0.1) and 50% ($f_{protected}$ = 0.5) of the landscape area to be protected while the remaining forest area is prone to deforestation (*FRAG*). Forest areas affected by deforestation in both models were simulated using a deforestation rate of d = 0.51% per year in America[1].